Supporting Information

Arnoldussen et al. 10.1073/pnas.1102984108

SI Materials and Methods

Visual Projection. Visual stimuli were projected by using an LCD projector (resolution, 1,280 × 1,024; InFocus) with custom-build optics. The image was projected, via a mirror, on a small (143 × 80.5 mm) projection screen, which was placed directly above the subjects' eyes (distance, ~3.0 cm). Subjects were able to focus on this short distance by wearing an individually designed soft convex lens with a refractive power of approximately +30 diopter. When needed, the refractive power was adjusted for the subjects' own refractive error (as assessed by an optician). Subjects wore the lens only in the left eye; the right eye was covered. This arrangement provided visual stimuli with an FOV of approximately 120 × 90°.

Before scanning the position of the rotation point of the subject's left eye was determined by using a previously described calibration procedure (1). During pursuit trials, the lateral displacement of the nodal point (2), which is located 6 mm in front of the rotation point, was taken into account for the correct projection of the flow field on the display screen.

Pursuit Accuracy. We measured pursuit accuracy in an additional control experiment in four of our subjects (subjects 1, 4, 5, and 6). Subjects wore a scleral induction coil in the left eye. The contact lens was carefully placed on top of the eye inside the opening of the scleral coil. The right eye was covered. Eye movements were measured while subjects viewed a sequence of pursuit conditions of 36 s each (i.e., twice as long as in the main experiment). This was done within a dummy scanner by using the same projection system as in the main experiment. All pursuit conditions used in the GLM (OPPONENT and CONSISTENT; 5 °/s and 10 °/s) and all axes of rotation [right anterior-left posterior semi-circular canal (RALP), left anterior-right posterior semi-circular canal (LARP), and vertical (VERT)] were included. Saccades were removed from the data before further analysis. Gain and phase difference of the smooth pursuit eye movements were calculated for each subject for each condition (Table S4). The results confirm our claim that smooth pursuit was accurate. Thus, we believe our conclusion that the phase relation between pursuit and retinal flow is the main determinant of the responses in the head-centric subregions stands. Even at the lowest gains (0.75), the difference in retinal speed is less than 5 °/s between the consistent and the opponent pursuit conditions, which is small compared with the range of speeds (20 °/s) used for retinal speed testing. However, we found little if any retinal speed sensitivity in precisely the head-centric flow regions (when tested with the full range of retinal speeds). Clearly, this reasoning holds a fortiori for the conditions with pursuit gain of 0.95. Our observations confirm and extend the control experiments reported previously (3) to pursuit during simulated head-centric flow about RALP and LARP axes.

GLM Model. The model consisted of five predictor variables and a constant as follows:

$$Y(t) = \beta_1 * Fb(t) + \beta_2 * Rs(t) + \beta_3 * Ps(t) + \beta_4 * Hs(t) + \beta_5 \quad \textbf{[S1]}$$

The first term (Fb) models a default flow response as a constant signal change in every motion condition compared with the static control condition. The second term (Rs) models the three speed levels of retinal rotational flow (5, 10, and 20 °/s). Hs models the four speed levels of head-centric rotational flow (0, 5, 10, and 20 °/s). Ps models the contribution of pursuit speed to the BOLD signal (0, 5, 10, and 20 °/s). The fifth β reflects a constant. The parametric predictors were de-meaned to ensure that the flow baseline predictor is orthogonal with respect to each parametric predictor. After collection of approximately one fifth of the experimental data, we decided to exclude the consistent condition at the highest Rs and Ps level (C_{20}) from all analyses and subsequent experimental runs for two reasons. In our view, accurate pursuit could not be guaranteed at this speed level. Poor pursuit would distort the retinal flow pattern to an unacceptably high level compared with the matching fixation condition (F_{20}) and causes significant retinal slip of the fixation target. Second, the GLM results without the C_{20} condition showed a decrease of the autocorrelation for the model. In those runs that included the C_{20} condition, we effectively excluded it from the analysis by modeling it as a separate dummy variable $\beta_6 * C_{20}(t)$ that is added to the GLM model while removing C_{20} from the other predictors.

Functional Localizers. For the MST localizer, a blocked design was used. Full-field flow, flow in the ipsilateral hemifield, flow in the contralateral hemifield, and a rest condition (static random dot pattern) were alternated. In the ipsi- and contralateral flow conditions, the flow was presented at 15° eccentricity and beyond, simulating a forward motion of 2 m/s. The remainder of the visual field was filled with a static random dot pattern.

The contrast between the full-field flow and the rest condition defined the MT^+ complex. MT and MST were defined as subregions of MT^+. Area MST was defined as all of the contiguous voxels that responded to ipsilateral flow presentation (4, 5). Area MT was defined as a region containing contiguous voxels that responded to contralateral, but not ipsilateral, flow.

To demarcate visual areas V1 to $V6^+$, we performed retinotopic mapping by using standard techniques (6). The polar angle mapping consisted of two runs. The subject was asked to fixate at the central fixation cross while a "wedge" stimulus of flow expanding from the fixation point (wedge width, 60°) moved clockwise over the visual field at one revolution in 36 s. The eccentricity mapping consisted of one run in which the subject maintained straight ahead fixation while a radial moving ring of flow moved from inner to outer visual field (maximum eccentricity, 60°) at a speed of 2 °/s. Both wedge shape and eccentricity ring were scaled by eccentricity in accordance with the cortical magnification factor and were surrounded by static dots against a dark background. The flow presented in the wedge and the ring was simulating forward movement of the eye at 1.5 m/s through a cloud of dots as in the main experiment.

The retinotopic data were analyzed by a cross-correlation analysis between BOLD activation and the phase of the stimulus. Phase direction reversals were taken as the borders of the main visual areas, and drawn by eye on a phase-colored data depiction on a flat map representation of each subject's anatomy. Area $V6^+$ was defined as a region medial to V3A that contained a representation of the entire contralateral visual field and an eccentricity map (7). In all subjects, $V6^+$ was located on the posterior branch of the parietooccipital sulcus. In macaque monkeys, V6 is bordering on a visual area with less clear retinotopic structure (i.e., V6A). In humans, the distinction between V6 and V6A is yet unresolved. Following an earlier suggestion (7), we denote our area of interest in the posterior branch of POS as the V6 complex ($V6^+$). We denoted MT+, V3A, and $V6^+$ as our ROIs, and restricted further analysis to voxels within these areas.

Nomenclature. The Talairach coordinates for Hs region within MST [average, (43, −59, 6)] are consistent with the pHFR found previously using a similar set of stimuli [average, (43, −63, 3) (3)]. This result shows the robustness of the finding that a subregion MST is modulated by head-centric signals for three axes of rotation. Our finding of pursuit modulation within MST is in line with single-cell recordings in Macaque monkeys (8, 9), as are pursuit signals within MT (8–11). The more posterior part of the Ps region within MST [average Talairach coordinates (44, −64, 0) corresponds well to the lateral pursuit modulated region found by Goossens et al. (3) (average Talairach coordinates (47, −67, −1)]. Perhaps this region is the human homolog of the lateral MST area in the monkey that was reported to respond to the motion of objects in a world frame (12) by integration of visual slip, eye pursuit, and vestibular signals. A general modulation by smooth pursuit eye movement within V3A has also been found previously (13).

Overall, we found no correlation among the retinotopic maps of V3A, V6$^+$, and MT and the location of the identified regions. Recently, human homologies of area FST, V4t, and PIT have been suggested within the MT$^+$ complex, using a more extensive retinotopy analysis (14). Given the large area estimation of our MT and MST (e.g., 960 mm^2 and 580 mm^2, respectively, for subject 2), it can be assumed that our MT$^+$ includes these satellite regions. Also, our V6$^+$ might comprise human homologies of both V6 and V6A (7). On the contrary, distinct neuronal populations might underlie the BOLD modulations we observed in the experimental sessions and the BOLD modulation for the retinotopy localizers.

Other Motion-Sensitive Areas. We looked into the responsiveness of five additional areas previously associated with processing of self-motion information: p2v, putative VIP (pVIP), parietoinsular vestibular cortex (PIVC), CSv, and pc (15). For each subject, all regions were identified with a GLM contrast between responses to the flow conditions and the static conditions in all runs that included the respective area. For all subjects, the minimal number of runs was 12, including four runs of each axis of rotation. Regions were identified on the inflated representation of the right hemisphere (Talairach coordinates in Table S3). For each region, we used a cluster threshold of 25 mm^2 and increased statistical threshold up to the level that showed a significant voxel population about this size ($P < 0.05$). Subsequently, β-values were obtained for the three parametric predictors, which were averaged over all subjects. Subsequent t tests revealed a significant deviation from zero of Hs_p2v, Hs_pVIP, Ps_CSv, and Ps_pc (Fig. S3).

1. van den Berg AV (1996) Judgements of heading. *Vision Res* 36:2337–2350.
2. Steinman RM, Cushman WB, Martins AJ (1982) The precision of gaze. A review. *Hum Neurobiol* 1:97–109.
3. Goossens J, Dukelow SP, Menon RS, Vilis T, van den Berg AV (2006) Representation of head-centric flow in the human motion complex. *J Neurosci* 26:5616–5627.
4. Dukelow SP, et al. (2001) Distinguishing subregions of the human MT+ complex using visual fields and pursuit eye movements. *J Neurophysiol* 86:1991–2000.
5. Huk AC, Dougherty RF, Heeger DJ (2002) Retinotopy and functional subdivision of human areas MT and MST. *J Neurosci* 22:7195–7205.
6. Sereno MI, et al. (1995) Borders of multiple visual areas in humans revealed by functional magnetic resonance imaging. *Science* 268:889–893.
7. Pitzalis S, et al. (2006) Wide-field retinotopy defines human cortical visual area v6. *J Neurosci* 26:7962–7973.
8. Chukoskie L, Movshon JA (2009) Modulation of visual signals in macaque MT and MST neurons during pursuit eye movement. *J Neurophysiol* 102:3225–3233.
9. Bremmer F, Ilg UJ, Thiele A, Distler C, Hoffmann KP (1997) Eye position effects in monkey cortex. I. Visual and pursuit-related activity in extrastriate areas MT and MST. *J Neurophysiol* 77:944–961.
10. Newsome WT, Wurtz RH, Komatsu H (1988) Relation of cortical areas MT and MST to pursuit eye movements. II. Differentiation of retinal from extraretinal inputs. *J Neurophysiol* 60:604–620.
11. Squatrito S, Maioli MG (1997) Encoding of smooth pursuit direction and eye position by neurons of area MSTd of macaque monkey. *J Neurosci* 17:3847–3860.
12. Ilg UJ, Schumann S, Thier P (2004) Posterior parietal cortex neurons encode target motion in world-centered coordinates. *Neuron* 43:145–151.
13. Brandt SA, et al. (1999) Sensory and motor components of smooth pursuit eye movements in extrastriate cortex. In *Current Oculomotor Research*, eds Becker W, Deubel H, Mergner T (Plenum, New York), pp 213–233.
14. Kolster H, Peeters R, Orban GA (2010) The retinotopic organization of the human middle temporal area MT/V5 and its cortical neighbors. *J Neurosci* 30:9801–9820.
15. Cardin V, Smith AT (2010) Sensitivity of human visual and vestibular cortical regions to egomotion-compatible visual stimulation. *Cereb Cortex* 20:1964–1973.

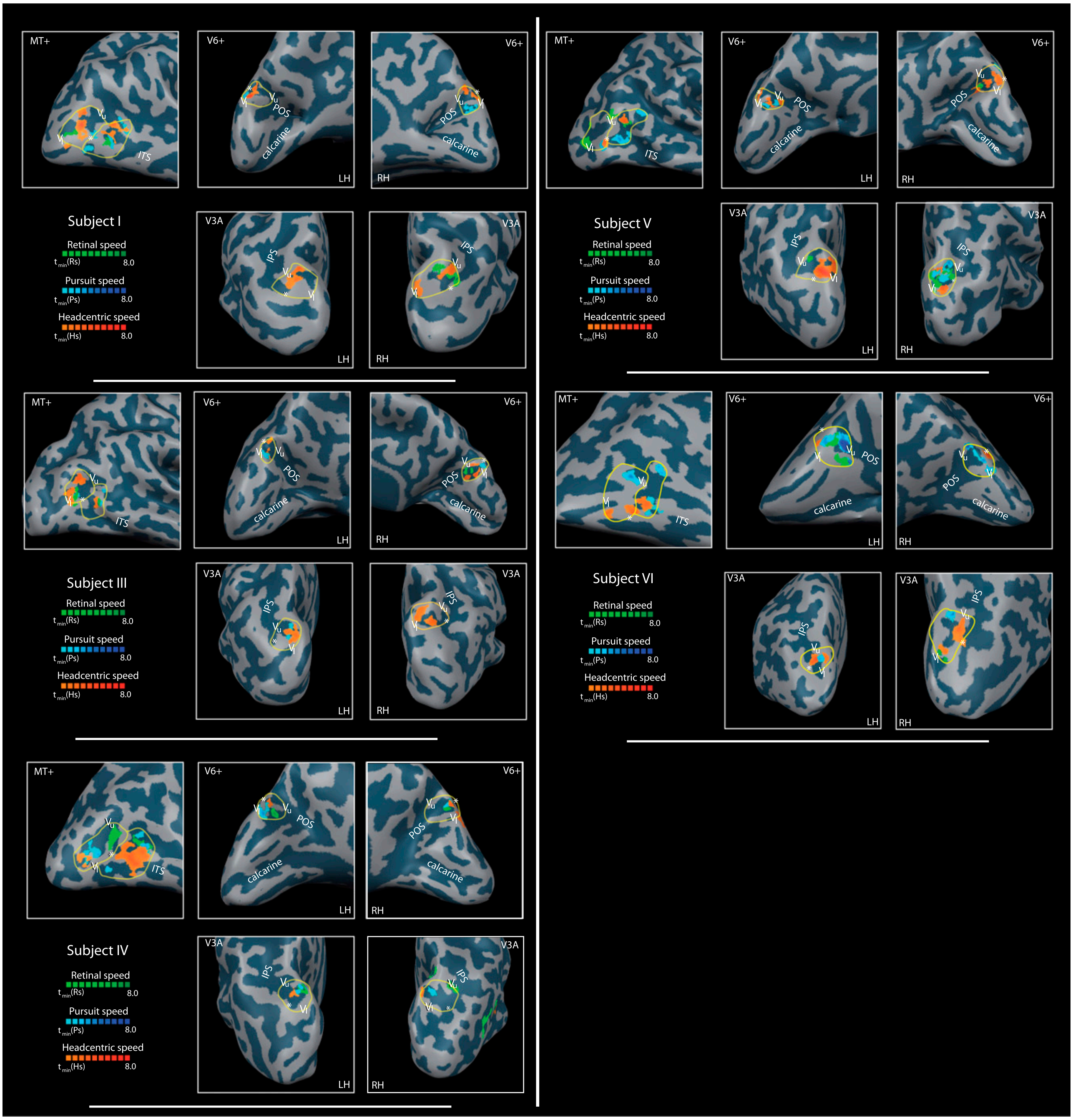

Fig. S1. Results for MT$^+$, MST, V3A, and V6$^+$ for the five remaining subjects in a similar format as Fig. 3. In all subjects, we consistently found subregions that showed a near-linear modulation related to the Rs, Ps, and Hs. Inspection of the results for data from different sessions for the two most scanned subjects showed that the location of these subregions was stable. Accompanying values for the t-min(Rs), t-min(Ps), and t-min(Hs) are listed in Table S1. Talairach coordinates of the identified Rs-, Ps-, and Hs-sensitive regions are listed in Table S2.

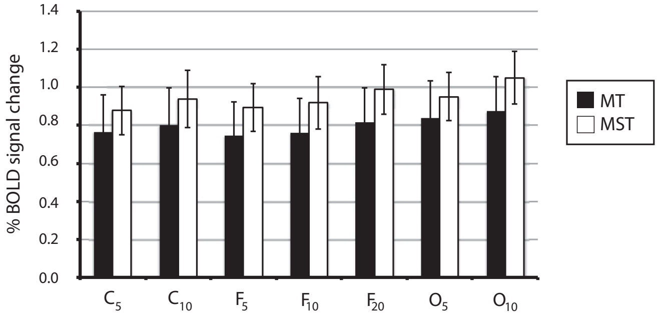

Fig. S2. Percent BOLD signal change on each of the seven individual conditions, for area MT and MST, averaged over all subjects. Error bars represent SEM.

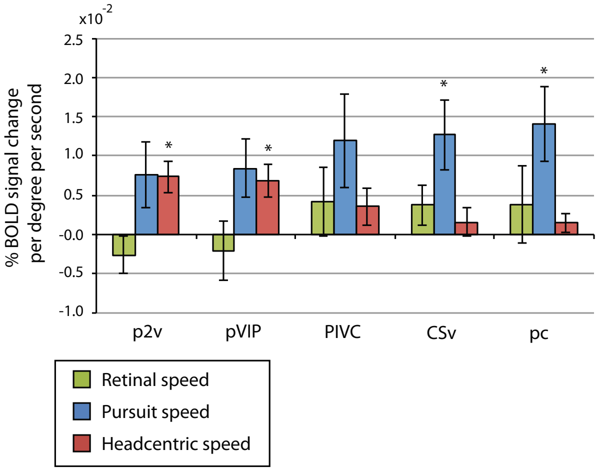

Fig. S3. Results of a global analysis of additional flow-responsive regions: p2v, pVIP, PIVC (not shown), CSv, and pc. (For a discussion of these areas, see ref. 14). For four of these areas, the response specificity to retinal speed, pursuit speed, and head-centric speed is plotted. P2v and pVIP are significantly modulated by head-centric speed; Csv and pc are significantly modulated by pursuit speed ($*P < 0.05$). PIVC did not reach significance on Rs, Ps, or Hs.

Table S1. **Selected *t* values for all regions for all ROIs**

	Subject					
t Value/predictor	I	II	III	IV	V	VI
RH						
MT+						
Hs	2.7	6.0	4.4	4.4	3.3	5.7
Ps	2.6	2.5	2.3	2.6	3.3	4.6
Rs	2.7	3.0	2.0	2.6	2.0	—
V3A						
Hs	3.5	2.7	4.0	5.2	3.6	4.0
Ps	—	2.7	—	5.5	2.8	4.4
Rs	2.2	2.7	—	3.2	2.1	2.0
V6+						
Hs	4.0	2.7	4.0	3.7	3.0	5.3
Ps	3.0	5.5	3.1	3.4	2.5	3.0
Rs	—	3.0	—	4.5	—	—
LH						
V3A						
Hs	4.5	3.5	4.5	3.6	4.0	4.0
Ps	—	2.5	—	3.4	3.0	5.5
Rs	—	2.5	3.0	2.5	—	—
V6+						
Hs	5.0	3.0	3.5	3.5	3.2	2.2
Ps	2.5	4.0	2.5	3.5	2.9	6.0
Rs	—	4.0	—	3.5	—	2.8

Threshold t-values for the identified Rs-, Ps-, and Hs-sensitive regions in Fig. S1.

Table S2. Talairach coordinates of the center of identified areas

	Rs			Ps$_{\text{post.}}$			Ps$_{\text{ant.}}$			Hs		
Area/subject	*x*	*y*	*z*	*x*	*y*	*z*	*x*	*y*	*z*	*x*	*y*	*z*
RH												
MST												
1	41	−56	8	48	−54	−6	45	−52	0	41	−50	0
2	52	−55	−5	52	−62	5	37	−55	9	48	−59	7
3	39	−71	10	47	−64	2	50	−63	9	42	−62	3
4	40	−58	10	39	−73	0	39	−58	8	40	−61	2
5	39	−64	13	36	−65	0	42	−54	14	41	−64	16
6	—	—	—	43	−62	1	42	−61	14	42	−63	1
Mean	42	−61	7	44	−63	0	43	−57	9	42	−60	5
MT*												
1	36	−74	1	48	−62	5	—	—	—	38	−68	4
2	41	−67	9	34	−76	6	—	—	—	42	−75	2
3	33	−85	6	37	−70	9	—	—	—	39	−74	8
4	44	−67	11	38	−76	5	—	—	—	34	−80	−1
5	24	−80	−3	39	−79	−2	—	—	—	39	−77	−1
6	—	—	—	42	−64	15	—	—	—	40	−79	2
Mean	35	−75	5	40	−71	6	—	—	—	39	−76	2
V3A*												
1	20	−88	17	—	—	—	—	—	—	21	−83	26
2	21	−78	21	29	−82	22	—	—	—	27	−82	35
3	—	—	—	—	—	—	—	—	—	13	−85	32
4	19	−83	24	14	−79	24	—	—	—	10	−83	32
5	18	−82	15	14	−84	13	—	—	—	11	−88	29
6	15	−84	23	17	−80	30	—	—	—	18	−74	21
Mean	19	−83	20	19	−81	22	—	—	—	17	−83	29
V6+*												
1	15	−73	21	13	−79	16	—	—	—	12	−77	26
2	14	−82	29	13	−72	36	—	—	—	13	−73	35
3	15	−76	28	17	−82	39	—	—	—	10	−78	32
4	18	−77	29	20	−80	31	—	—	—	20	−82	32
5	—	—	—	14	−83	35	—	—	—	13	−83	29
6	—	—	—	11	−74	38	—	—	—	19	−80	34
Mean	16	−77	27	15	−78	33	—	—	—	15	−79	31
LH												
V3A*												
1	—	—	—	—	—	—	—	—	—	−19	−93	22
2	−22	−87	26	−21	−85	21	—	—	—	−25	−83	17
3	−21	−81	24	—	—	—	—	—	—	−11	−86	22
4	−10	−82	28	−11	82	28	—	—	—	−18	−91	21
5	—	—	—	−10	−89	16	—	—	—	−8	−91	16
6	—	—	—	−13	−79	25	—	—	—	−15	−75	20
Mean	−18	−84	26	−14	−84	23	—	—	—	−16	−87	20
V6+*												
1	—	—	—	−15	−88	22	—	—	—	−17	−84	18
2	−17	−78	22	−10	−82	28	—	—	—	−4	−80	25
3	—	—	—	−10	−79	30	—	—	—	−12	−79	29
4	−12	−77	24	−5	−80	28	—	—	—	−13	−77	31
5	—	—	—	−8	−84	20	—	—	—	−18	−86	23
6	−10	−69	37	−11	−70	34	—	—	—	−11	−79	37
Mean	−13	−75	28	−10	−80	27	—	—	—	−13	−81	27

*Ps$_{\text{ant.}}$ and Ps$_{\text{post.}}$ values consolidated into Ps.

Table S3. Average Talairach coordinates of the center of the identified area averaged across all subjects

Area	*x*	*y*	*z*
p2v	27 (4)	−46 (10)	51 (5)
pVIP	23 (4)	−56 (5)	47 (4)
PIVC	56 (7)	−29 (4)	23 (7)
CSv	12 (2)	−21 (5)	40 (2)
Pc	12 (3)	−43 (5)	44 (5)

Values in parentheses are SDs.

Table S4. Results for pursuit accuracy measures

Condition	Gain	Phase (°)
VERT		
C5	0.93 (0.08)	0.0 (2.9)
O5	0.89 (0.11)	−2.5 (1.3)
C10	0.77 (0.12)	−2.3 (1.3)
O10	0.74 (0.13)	−4.5 (5.2)
RALP+LARP		
C5	0.94 (0.10)	5.1 (3.4)
O5	0.96 (0.04)	0.4 (3.2)
C10	0.81 (0.09)	2.0 (2.1)
O10	0.81 (0.05)	−1.3 (3.3)

Averages across four subjects and all three axes of rotation are shown, with SDs in parentheses.